Development and Implementation of 3D Algorithm of Neutron Transport Solution Via 2D(MOC) /1D(NEM) Fusion Method

Abstract:

Progress in nuclear engineering, as a highly interdisciplinary field, along with evolution in computational software and hardware, gives authorization to 3D transport simulation of highly heterogeneous generation IV reactor cores, instead of 3D diffusion calculation. To improve the computational efficiency of 3D neutron transport, fusion methods(2D/1D) are being considered. These methods offer a lower computational cost compared to the common methods, in which the 3D neutron transport kernel is divided into two separate kernels for each radial and axial direction since the material heterogeneity is not the same in these two directions. In implemented 2D/1D method in this research, the Nodal Diffusion Expansion Method (NEM) is utilized as an axial kernel due to its lower computational cost. Meanwhile, the radial direction was analyzed using the Method of Characteristic (MOC) utilizing modular ray tracing as the transport kernel because of the higher heterogeneity in this direction. The implemented algorithm has been evaluated by simulating the well-known Takeda Model 1 benchmark.

Keyword: Fusion Method, 2D/1D, Nodal Expansion Method, Whole Core Transport

1. Introduction

New generations of Nuclear Power Plants, have more complicated reactor core designs, Cores loaded partially with mixed-oxide fuel (MOX), high burn-up loadings (long operation cycle), and cores with advanced fuel assembly (radially heterogeneous) and new control rod designs (axially heterogeneous) are extensively considered in the IV generation of nuclear power plants. Such heterogeneous cores have pronounced leakage and spatial flux gradients between the adjacent and unlike assemblies[1]. The solution methods for these new heterogeneous cores are the main concern in the field of numerical transport calculation. Despite the high accuracy and precision of 3D calculation, because of the high computational cost, both in terms of memory management and run time, it seems that the combination of methods mitigates these concerns. One of the methods used today for 3D calculations is the fusion method (2D/1D), which means that radial and axial solver have their separate kernels for the solution of neutron transport (Fig.1)[2]. This is because, in the radial and axial directions, the heterogeneity is not the same. In nuclear reactor cores, the structural heterogeneity along the radial direction is often more pronounced than the axial. On the other hand, in 3D mode, integrated kernels (3D-SN, 3D-MOC, etc.), despite high accuracy, have a high computational cost including memory management and high execution time[3, 4].

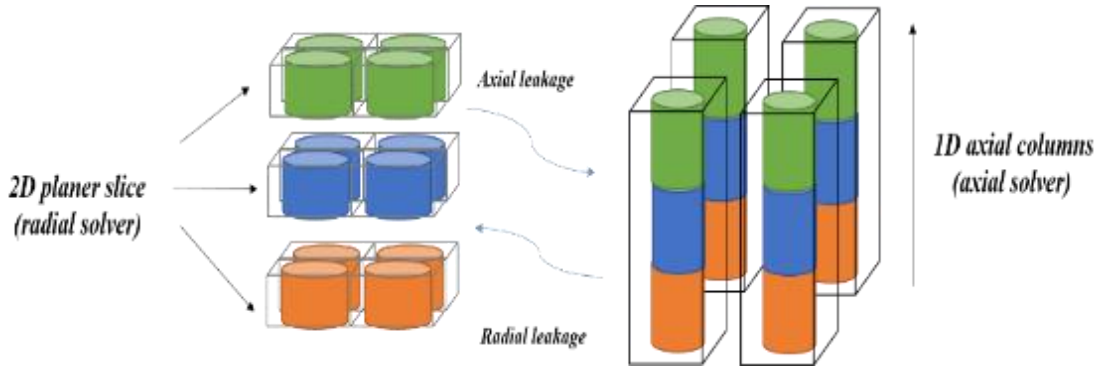

Fig.1: Flux leakage between axial and radial direction in 2D/1D fusion view

A common 2D/1D approach has been used with MOC as a planar solver in two dimensions and SN as an axial solver in one dimension, resulting in successful outcomes, so that the cost of calculations for structures with less axial heterogeneity could be significantly reduced. As the pioneer of the fusion method (2D/1D), CRX code developer uses the 2D/1D technique to implement 3D whole-core transport, in which MOC for radial 2-D calculation and the Diamond Difference (DD) scheme for axial 1-D calculation is applied[5, 6]. M.Hursin in his dissertation modified the

DeCART code axial solver that only provides a 1D axial solution based on the diffusion approximation whose accuracy depreciates in case of high neutron streaming. To mitigate this effect, he implemented a higher-order transport axial solver based on the NEM-SN derivation of the Boltzmann equation for a combination of nodal expansion and discrete ordinate methods[7]. S.Yuk and his colleagues solved neutron transport in a 2D/1D arrangement that is accelerated by the p-CMFD method. They provided a fine group library for their calculation[8]. Also, the 2D/1D method is implemented as transport solver in well-known MPACT code, in which Diffusion with NEM and SP_N with NEM are implemented as axial solvers[9]. Y.Zheng and his colleagues developed a 2D/1D code that utilized two different kernels for the axial and radial directions: the linear expansion is applied to the axial direction, then, the 3D solution of the angular flux is transformed to be the planar solution of 2D angular expansion moments, which are solved by the planar MOC sweeping[10]. For more detailed information about the 2D/1D technique, it can refer to mentioned references[2, 6, 11].

In the fusion method (2D/1D) presented in this research, MOC as the planar and Nodal Expansion Method (NEM) as axial solver, are developed and implemented. To implement MOC, there are two steps to follow. The first step involves covering the solution domain area or volume with lines, referred to as tracks. These tracks should be at a certain angle and with a specific spacing between adjacent parallel tracks. This is done to determine the necessary track density, generally covering solutions domain by using a series of lines with specified orientation and length is called ray-tracing [12](Fig.2). Since the structure of nuclear reactors consists of regular and repetitive geometries, it is possible to make ray-tracing calculations for a small cell (pin-cell) and propagate it to the entire core. This method is known as Modular Ray-Tracing (MRT), in this research a novel MTR developed in our previous research is updated for 2D/1D implemented method[13]. The prominent feature of this MRT is considerable reduction in required memory for 2D/1D simulation of reactor core. Second, the angular track average flux and scalar flux should be obtained by discretizing the hyperbolic transport equation in characteristic coordinates[4, 12]. NEM is used as an axial solver to expand flux in polynomials for solving the neutron diffusion equation. As a prominent feature of NEM, the flux of the current node is obtained from both adjacent nodes, this tight coupling relation is the cause of nodal capability for course mesh analysis. In this research, a new modified solver of 2D/1D as results of the combination of new MRT and NEM axial solver in which the heterogeneity in axial direction is preserved, is presented.

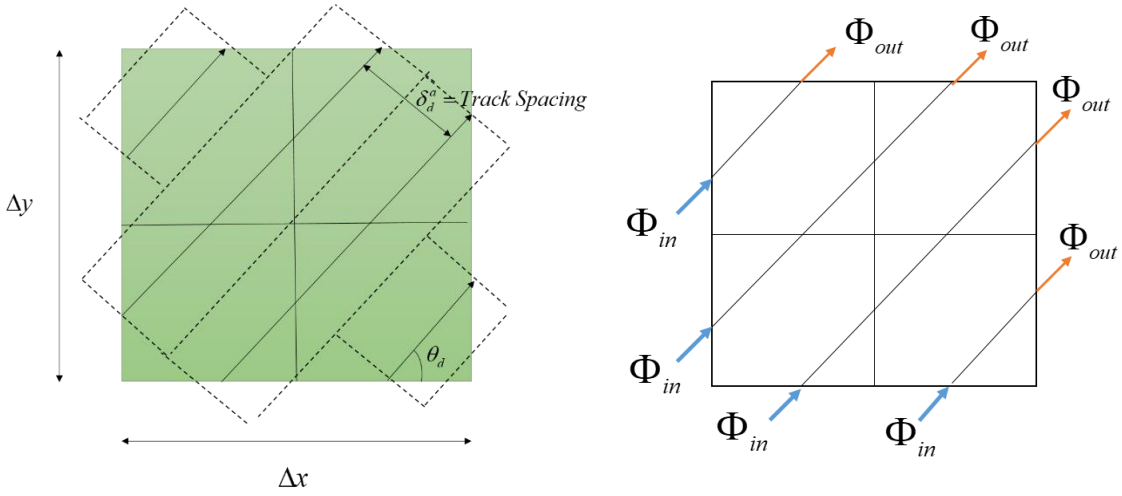

Fig.2: 2D unit cell discretization by ray tracing for MOC implementation[13, 14]

2. MOC Implementation

The derivation process of neutron transport along the characteristic line (s) is as follows, which is explained in detail in reference [4, 13, 15],

$$\frac{d\Phi_d^{i,g}}{ds_d} + \Sigma_{tr}^{i,g}\Phi_d^{i,g} = Q_d^{i,g} \qquad (1)$$

in which $\Phi_d^{i,g}$, $Q_d^{i,g}$ and $\Sigma_{tr}^{i,g}$ are angular flux, source term and transport cross section, also *i*, *d*, and g denote region, direction, and energy index, respectively. The solution is provided in Eq.(2). For simplicity, we designate: $\Phi_d^{i,g}(s_k) \rightarrow \Phi_{k,d}^{i,g}\big|_{out}$ and $\Phi_d^{i,g}(0) \rightarrow \Phi_{k,d}^{i,g}\big|_{in}$ in which *k* represents the track number.

$$\Phi_{k,d}^{i,g}\big|_{out} = \Phi_{k,d}^{i,g}\big|_{in} e^{-\Sigma_{tr}^{i,g}s_k} + \frac{Q_d^{i,g}}{\Sigma_{tr}^{i,g}}(1 - e^{-\Sigma_{tr}^{i,g}s_k}). \qquad (2)$$

In Eq.(2), the out and in indices refer to the outgoing and incoming angular flux to the track. As could be understood from Eq.(2), MOC as a discrete ordinate method requires an angular quadrature set to discretize the angular domain, which in this study a subroutine developed based on Legendre-Chebyshev quadrature set that produces angles and corresponding weights set , more details are available in reference [13].

2-1- Fusion (2D/1D) Method

The structure of the neutron transport equation, discretized concerning energy and angle, is as follows[8].

$$\vec{\Omega}_d.\nabla\Phi_d^g(r) + \Sigma_{tr}^g(r)\Phi_d^g(r) = q^g(\vec{r},\vec{\Omega}_n). \quad (3)$$

In the First step for the implementation of Eq.(3) in 2D/1D form, integrating Eq.(3) over $(z_{k+1/2}, z_{k-1/2})$ in the axial direction (z-direction), Eq.(4) is obtained. Eq.(4) is a two-dimensional equation (radial-direction) in which the net leakage of angular flux through the upper and lower nodes is taken into account.

$$\mu_d \frac{\partial}{\partial x}\Phi_{d,k}^g(x,y) + \eta_d \frac{\partial}{\partial y}\Phi_{d,k}^g(x,y) + \Sigma_{tr,k}^g(x,y)\Phi_{d,k}^g(x,y) = Q_{d,k}^g(x,y), \quad (4)$$

In this equation, source definition ($Q_{d,k}^g(x,y)$) is

$$Q_{d,k}^g(x,y) = q_{d,k}^g(x,y) - \frac{\varepsilon_d}{\Delta_k}[\Phi_{d,k+1/2}^g(x,y) - \Phi_{d,k-1/2}^g(x,y)]. \quad (5)$$

$$q_{d,k}^g(x,y) = \frac{1}{\Delta_k}\int_{z_{k-1/2}}^{z_{k+1/2}} dz q_d^g(x,y,z)\,, \Sigma_{tr,k}^g(x,y), \quad (6)$$

in which $\mu_d, \eta_d and\ \varepsilon_d$ are direction cosines. As can be seen from equation Eq. (5), the source term in this equation is modified by the axial incoming and outgoing angular flux at the node boundary.

Second, in this case, solving a one-dimensional equation is essential with a new source definition that is modified with the net radial leakage into the axial node.

To satisfy this expectation, we integrate Eq.(3) over $(x_{i-1/2,j}, x_{i+1/2,j})$ and$(y_{i,j-1/2}, y_{i,j+1/2})$, in the cell *(i, j, k)*, and by integrating the obtained relation along $(z_{k-1/2}, z_{k+1/2})$ in the cell (i, j, k) leads to

$$\frac{\varepsilon_d}{\Delta_k}(\Phi^g_{d,i,j,k+1/2} - \Phi^g_{d,i,j,k-1/2}) + \Sigma_{tr}{}^g_{,d,i,j,k}\Phi^g_{d,i,j,k} = Q^g_{d,i,j,k} \tag{7}$$

$$Q^g_{d,i,j}(z) = q^g_{d,i,j}(z) = \frac{\mu_d}{\Delta_i}(\Phi^g_{d,i+1/2,j}(z) - \Phi^g_{d,i-1/2,j}(z)) + \frac{\eta_d}{\Delta_j}(\Phi^g_{d,i,j+1/2}(z) - \Phi^g_{d,i,j-1/2}(z)) \tag{8}$$

the definitions for specified terms in the above equation are as follows

$$\Phi^g_{d,i,j,k\pm1/2} = \Phi^{g_{k\pm1/2}}_{d,i,j} \tag{9}$$

$$\Sigma_{\mathrm{tr}}{}^{\mathrm{g}}_{,\mathrm{d,i,j,k}} = \frac{1}{\Phi^{\mathrm{g}}_{\mathrm{n,i,j,k}}(\mathrm{z})}\frac{1}{\Delta_{\mathrm{k}}}\int_{\mathrm{z_{i-1/2}}}^{\mathrm{z_{i+1/2}}} \mathrm{dz}\Sigma_{\mathrm{tr}}{}^{\mathrm{g}}_{,\mathrm{d,i,j}}(\mathrm{z})\Phi^{\mathrm{g}}_{\mathrm{d,i,j}}(\mathrm{z})$$

$$= \frac{1}{\Phi^{\mathrm{g}}_{\mathrm{d,i,j,k}}(\mathrm{z})}\frac{1}{\Delta_{\mathrm{i}}\Delta_{\mathrm{j}}\Delta_{\mathrm{k}}}\int_{\mathrm{z_{i-1/2}}}^{\mathrm{z_{i+1/2}}} \mathrm{dz}\int_{\mathrm{x_{i-1/2}}}^{\mathrm{x_{i+1/2}}} \mathrm{dx}\int_{\mathrm{y_{j-1/2}}}^{\mathrm{y_{j+1/2}}} \mathrm{dy}\Sigma_{\mathrm{tr}}{}^{\mathrm{g}}(\mathrm{x,y,z})\Phi^{\mathrm{g}}_{\mathrm{d}}(\mathrm{x,y,z})\,. \tag{10}$$

Also, referring to Eq.(7) various solution methods are possible. If the heterogeneous configuration in the axial direction is divided into homogeneous segments, then the coefficient in Eq.(7) for each segment is constant and there is an exact solution for this equation at each segment.

Unlike the usual method in which the cell is homogenized in the axial direction[7], in this research the radial heterogeneity is preserved along the axial direction, Fig.3.

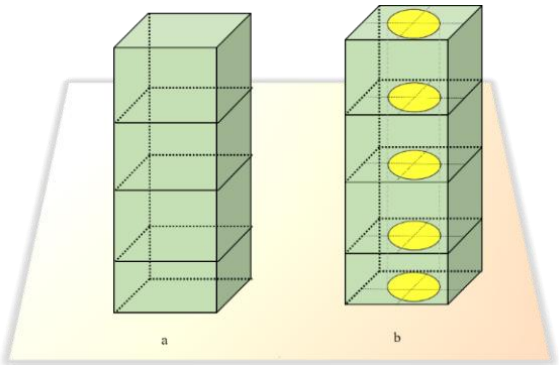

Fig.3. Axial cell configuration, a) homogenized cell, b) preserved heterogeneity.

In the common approach, due to homogenization, the solution speed is raised, but on the other hand, it loses some accuracy, especially when the heterogeneity of materials in a radial direction is high and the flux gradient for adjacent nodes is not negligible. In this research, by taking into account any radial node, *m*, Eq.(7) is changed to:

$$\varepsilon_d \frac{d}{dz} \Phi^g_{d,m}(z) + \Sigma^{\ g}_{tr,d,m}(z) \Phi^g_{d,m}(z) = Q^g_{d,m}(z), \tag{11}$$

The definitions for the specified terms in the above equation are as follows,

$$Q^g_{d,m}(z) = q^g_{d,m}(z) - L^g_{d,m}(z), \tag{12}$$

$$L^g_{d,m,k} = \int_{z_{k-\frac{1}{2}}}^{z_{k+\frac{1}{2}}} dz L^g_{d,m}(z) =$$

$$\frac{1}{A_m \Delta_k} \int_{z_{k-1/2}}^{z_{k+1/2}} dz \int_{A_m} dA\, \mu_d \frac{\partial}{\partial x} \Phi^g_d(x,y,z) + \eta_d \frac{\partial}{\partial y} \Phi^g_d(x,y,z) \tag{13}$$

$$= \frac{1}{A_m} \int_{A_m} dA \left(\mu_{d,k} \frac{\partial}{\partial x} \Phi^g_d(x,y) + \eta_d \frac{\partial}{\partial y} \Phi^g_{d,k}(x,y) \right),$$

in which A_m is defined as the area of radial sub-node, *m*. Also, in this equation $L^g_{d,m,k}$is the radial leakage into axial node k, and determined from Eq.(4) as follows,

$$L^g_{d,m,k} = \frac{1}{A_m} \int_{A_m} dA \left(\mu_{d,k} \frac{\partial}{\partial x} \Phi^g_d(x,y) + \eta_d \frac{\partial}{\partial y} \Phi^g_{d,k}(x,y) \right) \tag{14}$$

$$= Q^g_{d,m,k} - \Sigma^g_{tr,m,k} \Phi^g_{d,m,k}.$$

Although this method has a better-proven accuracy, it requires more memory during computing. Due to hardware and software capabilities, this problem can be resolved to a great extent.

As mentioned above, there are different solutions for the axial solver, Eq.(7). In what follows the NEM method is investigated as an axial solver. The following chart shows the general procedure for 2D/1D calculation in our implemented algorithm.

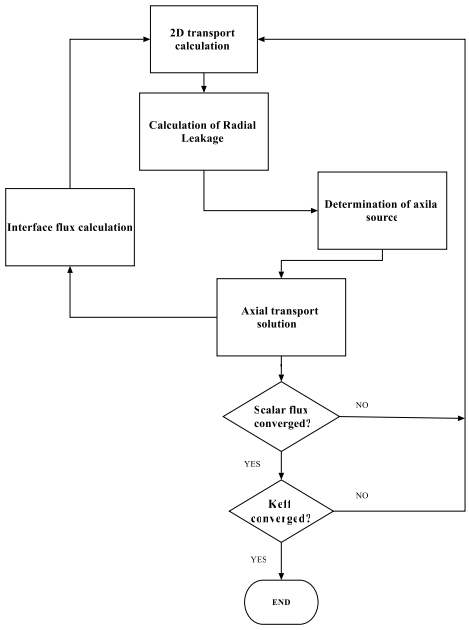

Fig.4. 2D/1D calculation procedure.

In the fusion 2D/1D method, the convergence criteria are applied to the final angular and scalar fluxes obtained from the axial kernel. As convergence criteria for two successive inner iterations, the 1.0E-5 is considered. Also, for outer iterations, the 1.0E-5 is applied.

2-2- Nodal Expansion Method (NEM) as Axial Solver

NEM is used as an axial solver to expand flux in polynomials for solving the neutron diffusion equation. NEM is known for its unique ability to derive a certain node flux from both adjacent nodes, which creates a strong coupling relationship and allows for effective course mesh analysis. Now we write the diffusion equation, in the following form,

$$-D\nabla^2\phi_g + \Sigma_{t,g}\phi_g = \sum_{g'=1}^{G} \Sigma_{sg'g}\phi_{g'} + \frac{\chi_g}{k_{eff}} \sum_{g'=1}^{G} \nu\Sigma_{fg'}\phi_{g'}. \qquad (15)$$

In which the parameters, diffusion coefficient(D), the total cross section (Σ_{tg}), fission cross section(Σ_{fg}), scattering cross-section ($\Sigma_{sg'g}$), neutron velocity(ν) and fission spectrum(χ_g) are defined. The solution domain in the z direction is subdivided into volumes centered on the points chosen to calculate the neutron flux. Fig.5 presents the node configuration for our NEM implementation.

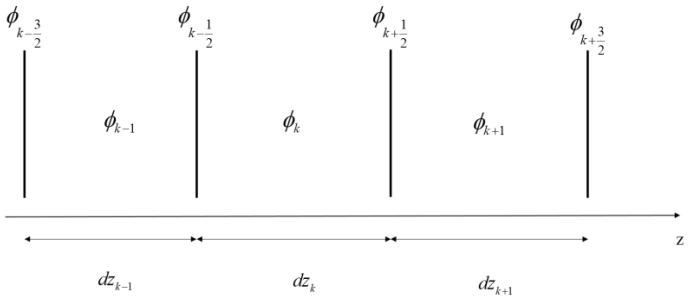

Fig.5. Flux on adjacent nodes and interface.

the following relation for flux at the node center is obtained.

$$\phi^g_{i,j,k} = \frac{w(\phi^g_{i,j,k+\frac{1}{2}} + \phi^g_{i,j,k-\frac{1}{2}}) + S}{2w + \Sigma_{t,g}} \quad , \quad w = \frac{4D^g_{i,j,k}}{(dz_k)^2} - \frac{\Sigma_{t,g}}{6}, \tag{16}$$

in which S as the source term represents the right-hand side of Eq.(15). As a result of current continuity at $k+\frac{1}{2}$ the edge, interface fluxes in terms of center node fluxes are obtained,

$$\phi^g_{i,j,k+\frac{1}{2}} = \frac{(4 - \frac{\phi^g_{i,j,k-\frac{1}{2}}}{\phi^g_{i,j,k}})\phi^g_{i,j,k}}{3(1+w)} + \frac{(4 - \frac{\phi^g_{i,j,k+\frac{3}{2}}}{\phi^g_{i,j,k+1}})\phi^g_{i,j,k+1}}{3(1+w)} \quad w = \frac{D^g_{i,j,k+1} dz_{i,j,k}}{D^g_{i,j,k} dz_{i,j,k+1}}. \tag{17}$$

When this edge is the boundary edge, we use the P1 approximation (linearly anisotropic flux) to calculate interface flux at the boundary edge(Fig.6).

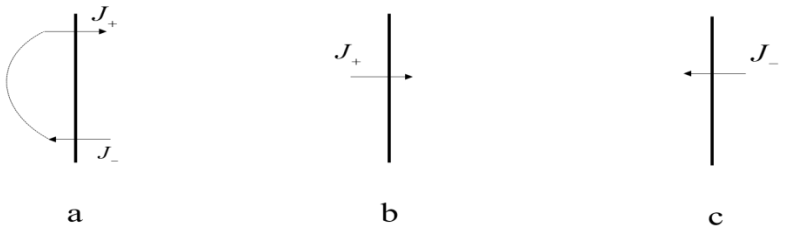

Fig.6. a) Reflecting boundary, b) Left boundary, c) Right boundary.

In particular, the interface flux for the left boundary is

$$\phi^g_{i,j,\frac{1}{2}} = \frac{(4 - \frac{\phi^g_{i,j,\frac{3}{2}}}{\phi^g_{i,j,1}})\phi^g_{i,j,1}}{(3 - \frac{dz_1 \beta}{D_1})}. \tag{18}$$

3. Results and Discussion

To verify the implemented algorithm, the Takeda Model 1 (TM1) a 3D benchmark is investigated. The investigated Kyoto University Critical Assembly (KUCA) benchmark includes a fissionable fuel, a control rod, and a reflector section, making it a small LWR core model[16]. The core arrangement is presented in Fig.7. As demonstrated in Fig.8, core symmetry in this benchmark provides a simulation with a reflecting boundary. Two energy groups for core calculations are considered (Table. 1). Also a detailed description of the cross-section are available in Appendix 3 of reference[16]. The following two cases are taken into account;

Case 1: The control rod is fully withdrawn (un-rodded-void) and, Case 2: The control rod is fully inserted (rodded).

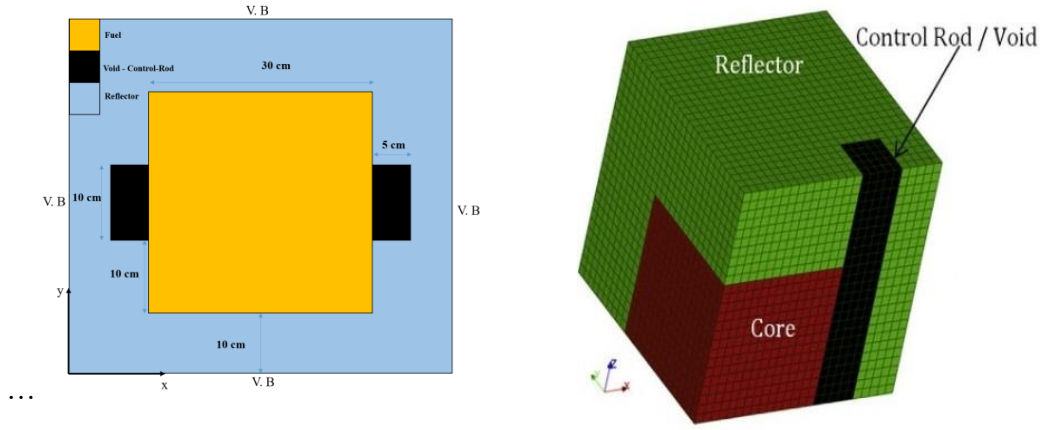

a) Whole Core with Four Vacuum Boundary Conditions b) 3D Reflected Core

Fig.7 . Core Configuration of TM1 Benchmark.

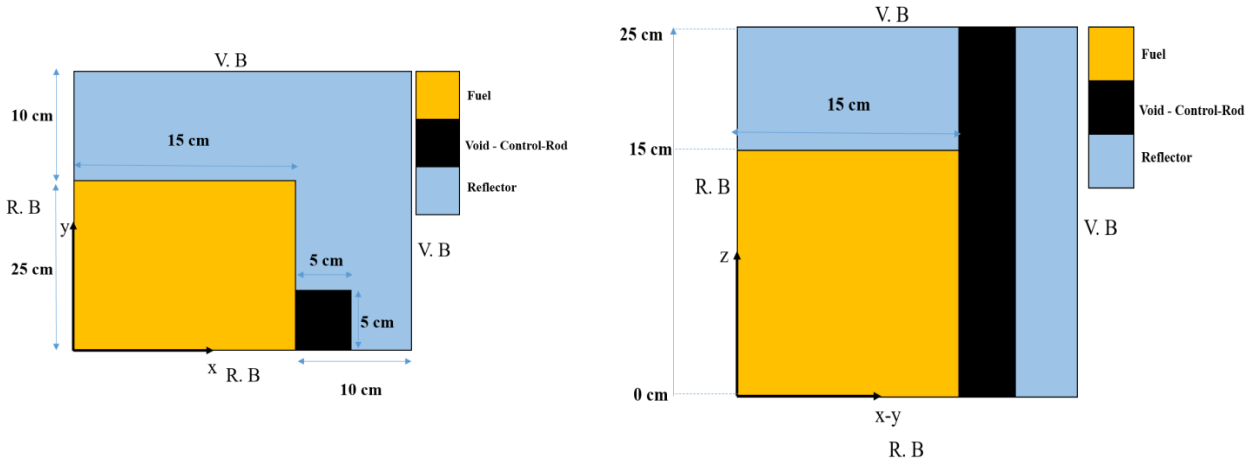

Radial core configuration

Axial core configuration

Fig.8. TM1 reflected core.

As mentioned, 2D/1D transport calculation utilizes the MOC and NEM as planar and axial kernels respectively. Therefore, regarding the planar kernel and modular mesh study presented in references[4, 15], pin-cell with dimensions of 0.5 cm x 0.5 cm and a track spacing of 0.05 cm is discretized by modular ray tracing. Moreover, in the axial direction, the 25 cm height of the model is divided into 50 meshes.

Table. 1. 2-group energy structure for small LWR

Group	Energy range (ev)		Fission Spectrum
	Lower	Upper	
1	1.0000E+7	6.8256E-1	1.0
2	6.8256E-1	1.0000E-5	0.0

2-1-TM1 Calculation Results

Computational Cost for 3D implementation of neutron transport for criticality calculation of presented benchmark shows that our implement 2D/1D requires 1320 MB RAM however 3D MOC entails 5255 MB ([4]), which demonstrates a considerable reduction in required memory. Since the optimization of the presented algorithm for convergence requires more modification, it is not reasonable to speak precisely about the execution time. Also Table.2 represents criticality calculation for the S_{12} angular order of Legendre-Chebyshev quadrature set for two cases un-rodded and rodded.

Table.2. The Multiplication Factor of TM1 Benchmark. (Legendre-Chebyshev quadrature set).

Method	case1 (k_{eff})	case 2 (k_{eff})	Case1 Δk_{eff}	case 2 Δk_{eff}
Reference	0.9780	0.9624	-	-
Fusion (2D/1D)	0.9755	0.9449	-0.00251	-0.01753

Also, region averaged scalar fluxes are presented in Table.3 and Table.4 for case 1 and case 2 of TM1 benchmark, respectively.

Table.3 . Region Averaged Scalar Flux for Case 1 of TM1. (Legendre-Chebyshev quadrature set).

Method	**Energy group**	**Core**		**Reflector**		**Void**	
		Average	**Diff (%)**	**Average**	**Diff (%)**	**Average**	**Diff (%)**
Reference	1	4.751E-03	-	5.925E-04	-	1.450E-03	-
	2	8.699E-04	-	9.140E-04	-	9.741E-04	-
2D/1D(NEM)	1	4.60E-03	-3.25	6.375E-04	7.05	1.701E-03	14.75
	2	8.769E-04	0.79	9.765E-04	6.40	1.046E-03	6.86

Table.4 . Region Averaged Scalar Flux for Case 2 of TM1. (Legendre-Chebyshev quadrature set).

Method	**Energy group**	**Core**		**Reflector**		**Control Rod**	
		Average	**Diff (%)**	**Average**	**Diff (%)**	**Average**	**Diff (%)**
Reference	1	4.913E-03	-	5.911E-04	-	1.225E-03	-
	2	8.692E-04	-	8.790E-04	-	2.460E-04	-
2D/1D(NEM)	1	4.811E-03	-2.10	6.289E-04	6.01	1.179E-03	-3.88
	2	8.703E-04	0.13	9.124E-04	3.66	2.590E-04	4.98

Presented results in Table.3 and Table.4 contain two points: First, it appears that the flux difference in the void region is greater than the flux difference in the control rod region between our implemented fusion kernel and the reference value. This greater difference in flux in the void region

between the two calculations emerges from the low scattering cross-section of the void region which leads to a ray effect phenomenon relative to the region containing the control rod. Second, when the control rod is fully inserted, a gradian of the flux in the vicinity of the control rod occurred due to the presence of materials with high heterogeneity in the absorption cross section. Therefore, to bring the simulation results closer to the reference values, it is necessary to provide finer meshes in the vicinity of the control rod.

4. Conclusions

In this research to investigate the neutron transport equation solution in 3D heterogeneous structures, a fusion method (2D/1D) is developed and a Fortran modular code is implemented, where MOC as planar and NEM as axial solver are integrated. The Takeda Model 1, a 3D benchmark in which three different materials are utilized in the core structure, is considered to evaluate our implemented algorithm. The implemented 2D/1D kernel in this research preserves radial heterogeneity of pin-cell in the axial direction, moreover respect to the 3D integrated MOC kernel, a noticeable reduction in usage memory is occurred. Obtained results for our implemented 2D/1D kernels show acceptable accuracy, however, these kernels need to be modified to have higher performance along the axial direction. The current discontinuity factor is the average current difference between two sides of a node in the axial direction, as a flatting factor is required for further improvement.

5. References

1. Pediz, G., A. Yılmazer, and M. Tombakoğlu, *Transport equivalent full core neutronics calculations via finite volume method and optimized diffusion parameters.* Progress in Nuclear Energy, 2023. **165**: p. 104935.
2. Larsen, E.W., et al., *MPACT Theory ManualVersion 4.3*. 2022, Oak Ridge National Lab.(ORNL), Oak Ridge, TN (United States).
3. Fitzgerald, A., *Parallel 3-D Method of Characteristics with Linear Source and Advanced Transverse Integration*. 2020.
4. Porhemmat, M., et al., *Developing 3D neutron transport kernel for heterogeneous structures in an improved method of characteristic (MOC) framework.* Progress in Nuclear Energy, 2020. **127**: p. 103442.
5. Lee, G. and N.-Z. Cho, *3-D Whole-Core Transport Calculations of the Extended OECD Benchmark Problem C5G7 MOX by the CRX Code.* TRANSACTIONS OF THE AMERICAN NUCLEAR SOCIETY, 2003. **89**: p. 271-271.

6. Lee, G.S. and N.Z. Cho, *2D/1D fusion method solutions of the three-dimensional transport OECD benchmark problem C5G7 MOX.* Progress in Nuclear Energy, 2006. **48**(5): p. 410-423.
7. Hursin, M., *Full core, heterogeneous, time dependent neutron transport calculations with the 3D code DeCART*. 2010: University of California, Berkeley.
8. Yuk, S. and N.Z. Cho, *Whole-core transport solutions with 2-D/1-D fusion kernel via p-CMFD acceleration and p-CMFD embedding of nonoverlapping local/global iterations.* Nuclear Science and Engineering, 2015. **181**(1): p. 1-16.
9. Collins, B., et al., *Stability and accuracy of 3D neutron transport simulations using the 2D/1D method in MPACT.* Journal of Computational Physics, 2016. **326**: p. 612-628.
10. Zheng, Y., S. Choi, and D. Lee, *A new approach to three-dimensional neutron transport solution based on the method of characteristics and linear axial approximation.* Journal of Computational Physics, 2017. **350**: p. 25-44.
11. Zin, C.N., *Fundamentals and recent developments of reactor physics methods.* Nuclear Engineering and Technology, 2005. **37**(1): p. 25-78.
12. Porhemmat, M., K. Hadad, and M. Mahzoon, *Modular ray tracing in 2D whole core transport with MOC.* Progress in Nuclear Energy, 2017. **99**: p. 103-109.
13. Porhemmat, M., et al., *Improved memory management for solving neutron transport via a novel Modular Ray Tracing (MRT) approach embedded in parallel method of characteristic (MOC) framework.* Progress in Nuclear Energy, 2021. **132**: p. 103590.
14. Porhemmat, M., et al., *Verification and validation of the modular ray tracing MOC using the coupled forward-adjoint approach and application to C5G7 benchmark.* Annals of Nuclear Energy, 2019. **129**: p. 13-20.
15. Kochunas, B.M., *A Hybrid Parallel Algorithm for the 3-D Method of Characteristics Solution of the Boltzmann Transport Equation on High Performance Compute Clusters*. 2013.
16. Takeda, T. and H. Ikeda, *3-D neutron transport benchmarks.* Journal of Nuclear Science and Technology, 1991. **28**(7): p. 656-669.